Modulation of Mammalian Inositol 1,4,5-Trisphosphate Receptor Isoforms by Calcium: A Role of Calcium Sensor Region

Huiping Tu, Zhengnan Wang, and Ilya Bezprozvanny
Department of Physiology, University of Texas Southwestern Medical Center at Dallas, Dallas, Texas 75390

ABSTRACT In the accompanying article, we compared main functional properties of the three mammalian inositol 1,4,5-trisphosphate receptors ($InsP_3R$) isoforms. In this article we focused on modulation of mammalian $InsP_3R$ isoforms by cytosolic Ca^{2+}. We found that: 1), when recorded in the presence of 2 μM $InsP_3$ and 0.5 mM ATP all three mammalian $InsP_3R$ isoforms display bell-shaped Ca^{2+} dependence in physiological range of Ca^{2+} concentrations (pCa 8–5); 2), in the same experimental conditions $InsP_3R3$ is most sensitive to modulation by Ca^{2+} (peak at 107 nM Ca^{2+}), followed by $InsP_3R2$ (peak at 154 nM Ca^{2+}), and then by $InsP_3R1$ (peak at 257 nM Ca^{2+}); 3), increase in ATP concentration to 5 mM had no significant effect of Ca^{2+} dependence of $InsP_3R1$ and $InsP_3R2$; 4), increase in ATP concentration to 5 mM converted Ca^{2+} dependence of $InsP_3R3$ from "narrow" shape to "square" shape; 5), ATP-induced change in the shape of $InsP_3R3$ Ca^{2+} dependence was mainly due to an >200-fold reduction in the apparent affinity of the Ca^{2+}-inhibitory site; 6), the apparent Ca^{2+} affinity of the Ca^{2+} sensor region (Cas) determined in biochemical experiments is equal to 0.23 μM Ca^{2+} for RT1-Cas, 0.16 μM Ca^{2+} for RT2-Cas, and 0.10 μM Ca^{2+} for RT3-Cas; and 7), Ca^{2+} sensitivity of $InsP_3R1$ and $InsP_3R3$ isoforms recorded in the presence of 2 μM $InsP_3$ and 0.5 mM ATP or 2 μM $InsP_3$ and 5 mM ATP can be exchanged by swapping their Cas regions. Obtained results provide novel information about functional properties of mammalian $InsP_3R$ isoforms and support the importance of the Ca^{2+} sensor region (Cas) in determining the sensitivity of $InsP_3R$ isoforms to modulation by Ca^{2+}.

INTRODUCTION

The inositol (1,4,5)-triphosphate receptor ($InsP_3R$) is an intracellular calcium (Ca^{2+}) release channel that plays a key role in Ca^{2+} signaling in cells (Berridge, 1993). Three mammalian $InsP_3R$ isoforms—$InsP_3R$ type 1 ($InsP_3R1$), $InsP_3R$ type 2 ($InsP_3R2$), and $InsP_3R$ type 3 ($InsP_3R3$)—are expressed in mammals (Furuichi et al., 1994), each with the unique expression pattern (Taylor et al., 1999). Modulation of $InsP_3R$ by cytosolic Ca^{2+} is one of the most fundamental $InsP_3R$ properties responsible for complex spatiotemporal aspects of Ca^{2+} signaling (Berridge, 1993). In the accompanying article (Tu et al., 2005), we used the planar lipid bilayer reconstitution technique to compare main functional properties (conductance, gating, $InsP_3$ sensitivity, and modulation by ATP) of the recombinant rat $InsP_3R1$, $InsP_3R2$, and $InsP_3R3$ expressed in Sf9 cells by baculoviral infection. In this article, we used the planar lipid bilayer reconstitution technique and biochemical experiments to compare modulation of mammalian $InsP_3R$ isoforms by cytosolic Ca^{2+}. In our previous studies, we identified a putative Ca^{2+} sensor region (Cas) within a modulatory domain of $InsP_3R1$ (Miyakawa et al., 2001; Tu et al., 2003). Here we show that the observed differences in Ca^{2+} sensitivity between mammalian $InsP_3R$ isoforms can be explained by isoform-specific differences in affinities of the Cas region for Ca^{2+}. Our results provide information about Ca^{2+} modulation of three mammalian $InsP_3R$ isoforms and further support a role of the Ca^{2+} sensor region (Cas) in the $InsP_3R$ modulation by Ca^{2+}.

MATERIAL AND METHODS

Generation of recombinant baculoviruses

The baculoviruses expressing rat $InsP_3R1$ (RT1) and rat $InsP_3R3$ (RT3) have been previously described (Maes et al., 2000; Tu et al., 2002). The generation of baculovirus encoding rat $InsP_3R2$ (RT2) is described in the accompanying article (Tu et al., 2005). The RT1-V-3 and RT3-V-1 chimeric constructs in pFastBac1 vector (Invitrogen, Carlsbad, CA) were generated by PCR-mediated gene fusion and verified by sequencing. In RT1-V-3 construct amino acids E1932-L2312 of $InsP_3R1$ were replaced with amino acids M1835-F2242 of $InsP_3R3$; in RT3-V-1 construct amino acids M1835-F2242 of $InsP_3R3$ were replaced with amino acids E1932-L2312 of $InsP_3R1$. The RT1-V-3 and RT3-V-1 baculoviruses were generated and amplified using Bac-to-Bac system according to the manufacturer's (Invitrogen) instructions. Expression of RT1-V-3 and RT3-V-1 proteins in Sf9 cells was confirmed by Western blotting with rabbit polyclonal anti-$InsP_3R1$ antibody T443 described previously (Kaznacheyeva et al., 1998) and the affinity purified rabbit polyclonal anti-$InsP_3R3$ antibody (IB7124-AP) described in the accompanying article (Tu et al., 2005).

Expression of $InsP_3R$ in Sf9 cells and planar lipid bilayer experiments

RT1, RT2, RT3 isoforms, RT1-V-3, and RT3-V-1 chimeras were expressed in Sf9 cells and reconstituted into planar lipid bilayers as described in the accompanying article (Tu et al., 2005). Single-channel analysis of currents supported by RT1-V-3 and RT3-V-1 chimeras was performed as described for RT1, RT2, and RT3 isoforms in the accompanying article (Tu et al., 2005). Ca^{2+} dependence of $InsP_3R$ isoforms and chimeras was determined

Submitted July 14, 2004, and accepted for publication October 29, 2004.

Address reprint requests to Dr. Ilya Bezprozvanny, Dept. of Physiology, K4.112 UT Southwestern Medical Center at Dallas, 5323 Harry Hines Blvd., Dallas, TX 75390-9040. Tel.: 214-648-6737; Fax: 214-648-2974; E-mail: ilya.bezprozvanny@utsouthwestern.edu.

0006-3495/05/02/1056/14 $2.00

doi: 10.1529/biophysj.104.049601

as described in Bezprozvanny et al. (1991) by consecutive additions $CaCl_2$ to the *cis* (cytosolic) chamber from the concentrated 20 mM $CaCl_2$ stock with at least 30 s stirring of solutions in both chambers. Calcium concentration in 20 mM $CaCl_2$ stock solution was verified by atomic absorption spectroscopy (Galbraith Laboratories, Knoxville, TN). Free Ca^{2+} concentration in the *cis* chamber was controlled in the range from 10 nM Ca^{2+} (pCa 8) to 100 μM Ca^{2+} (pCa 4) by the mixture of 1 mM EGTA, 1 mM HEDTA, and variable concentrations of $CaCl_2$ and calculated by using a program described in Fabiato (1988). Evidence for the presence of multiple channels in the bilayer (multiple open levels) was obtained in the majority of the experiments. The single-channel open probability (*Po*) was estimated from multichannel records and normalized to the maximum *Po* observed in the same experiment as described for $InsP_3$- and ATP-dependence experiments in the accompanying article (Tu et al., 2005). The normalized data from several experiments with each $InsP_3R$ isoform or chimera were averaged together for presentation and fitting as described for $InsP_3$- and ATP-dependence experiments in the accompanying article (Tu et al., 2005).

To obtain parameters of Ca^{2+} dependence the normalized and averaged data were fit by the ''bell-shaped equation'':

$$P(Ca^{2+}) = 4P_m k_{Ca}^n [Ca^{2+}]^n / ((k_{Ca}^n + [Ca^{2+}]^n)(K_{Ca}^n + [Ca^{2+}]^n)), \quad (1)$$

modified from Bezprozvanny et al. (1991), where P_m is a parameter proportional to the maximal normalized *Po* value, *n* is the Hill coefficient, K_{Ca} is the apparent affinity of the Ca^{2+}-activating site, and k_{Ca} is the apparent affinity of the Ca^{2+}-inhibitory site. As explained in Tu et al. (2003), parameter P_m is equal to maximal normalized *Po* only in the case when $k_{Ca} = K_{Ca}$. If $k_{Ca} \neq K_{Ca}$, parameter *Po* is proportional (and higher) than maximal *Po*.

To obtain parameters of Ca^{2+} dependence of $InsP_3R3$ and RT1-V-3 at 5 mM ATP, the normalized and averaged data were fit by the ''biphasic Hill equation'':

$$P(Ca^{2+}) = P_m / ((1 + (K_{Ca}/[Ca^{2+}])^{Ha})(1 + ([Ca^{2+}]/k_{Ca})^{Hi})), \quad (2)$$

modified from Mak et al. (1998), where P_m is a parameter proportional to the maximal normalized *Po* value, *Ha* is the Hill coefficient of the activation phase, K_{Ca} is the apparent affinity of the Ca^{2+}-activating site, *Hi* is the Hill coefficient of the inhibitory phase, and k_{Ca} is the apparent affinity of the Ca^{2+}-inhibitory site.

The fits using Eqs. 1 and 2 were generated using least-squares routine (Sigma Plot 2001, Jandel Scientific) and the quality of the fit was evaluated from the coefficient of determination (R^2). The standard errors of resulting parameters were obtained as the estimates of the uncertainties in the values of regression coefficients obtained as a result of the fitting procedure (Sigma Plot 2001, Jandel Scientific, San Rafael, CA).

Ca^{2+} binding assay

RT1-Cas (E1932-R2270 of rat $InsP_3R1$) expression construct in pGEX-KG expression vector (Amersham-Pharmacia Biotech, Uppsala, Sweden) was previously described (Tu et al., 2003). RT2-Cas (E1884-R2224 of rat $InsP_3R2$) and RT3-Cas (M1835-R2199 of rat $InsP_3R3$) regions were amplified by polymerase chain reaction (PCR) and subcloned into pGEX-KG vector. RT1-Cas, RT2-Cas, and RT3-Cas proteins were expressed in BL21 bacteria, purified on glutathione-sepharose 4B beads (Amersham-Pharmacia Biotech), and cleaved from glutathione *S*-transferase (GST) by thrombin as previously described for RT1-Cas (Tu et al., 2003). Obtained proteins were used immediately in intrinsic tryptophan fluorescence spectroscopy measurements performed as previously described for RT1-Cas (Tu et al., 2003). Briefly, a quartz cuvette containing 2 ml of recombinant proteins at 80 μg/ml in *cis* recording buffer (110 mM Tris dissolved in HEPES, pH 7.35) was supplemented with 1 mM EGTA and 1 mM HEDTA (pH 7.35). The free Ca^{2+} concentration in the cuvette was adjusted in the range pCa 9.4–2 by consecutive additions of calibrated $CaCl_2$ stock solutions (20 mM $CaCl_2$, 100 mM $CaCl_2$, and 1 M $CaCl_2$) with constant stirring. The free Ca^{2+} concentration in the cuvette was calculated using MaxChelator (http://www.stanford.edu/~cpatton/maxc.html). Intrinsic tryptophan fluorescence was excited by 280 nm (2-nm-slit width) light (DeltaRAM, Photon Technology International, Lawrenceville, NJ) and emission spectra were collected at room temperature in the 290–500-nm range with a 2-nm step size. The experiments were controlled and analyzed by Felix software package (Photon Technology International).

The absolute peak tryptophan fluorescence values at each Ca^{2+} concentration $F(Ca^{2+})$ were determined from the generated emission spectra. The measured peak fluorescence values were corrected for dilution $F_{cor}(Ca^{2+}) = F_0/(1 + v/V)$, where $F_{cor}(Ca^{2+})$ is dilution-corrected peak fluorescence value, F_0 is the peak fluorescence value with no $CaCl_2$ added (pCa 9.4), *v* is the total volume of $CaCl_2$ added, and *V* is the starting solution volume in the cuvette (2 ml). The difference between measured and dilution-corrected peak tryptophan fluorescence values $\Delta F(Ca^{2+}) = F(Ca^{2+}) - F_{cor}(Ca^{2+})$ was taken as a measure of Ca^{2+}-induced conformational changes in RT1-Cas, RT2-Cas, and RT3-Cas recombinant proteins (Tu et al., 2003; Ward, 1985). The ΔF values at each Ca^{2+} concentration were normalized to the maximal ΔF value (ΔF_{max}) measured at pCa 2.0 in the same experiment. The normalized ΔF values from three independent experiments for each recombinant protein were averaged together at each Ca^{2+} concentration for presentation and fitting. The Ca^{2+} dependence of the normalized and averaged ΔF values was fit using equation

$$\Delta F/\Delta F_{max}(Ca^{2+}) = [Ca^{2+}]^n / ([Ca^{2+}]^n + K_{Ca}^n), \quad (3)$$

from Tu et al. (2003), where $[Ca^{2+}]$ is the Ca^{2+} concentration in the cuvette, *n* is the Hill coefficient, and K_{Ca} is the apparent affinity for Ca^{2+}. The fits were generated using least-squares routine (Sigma Plot 2001, Jandel Scientific), and the quality of the fit was evaluated from the coefficient of determination (R^2). The standard errors of resulting K_{Ca} and *n* values were obtained as the estimates of the uncertainties in the values of regression coefficients obtained as a result of the fitting procedure (Sigma Plot 2001, Jandel Scientific).

RESULTS

Modulation of mammalian $InsP_3R$ isoforms by Ca^{2+}

In the accompanying article (Tu et al., 2005), we compared main functional properties (conductance, gating, $InsP_3$ sensitivity, and modulation by ATP) of the recombinant rat $InsP_3R1$, $InsP_3R2$, and $InsP_3R3$ expressed in Sf9 cells by baculoviral infection and reconstituted into planar lipid bilayers. Modulation of $InsP_3R$ by cytosolic Ca^{2+} is one of the most fundamental $InsP_3R$ properties responsible for complex spatiotemporal aspects of Ca^{2+} signaling (Berridge, 1993). Does cytosolic Ca^{2+} affect $InsP_3R$ function in an isoform-specific manner? To answer this question we determined Ca^{2+} dependence of recombinant $InsP_3R1$, $InsP_3R2$, and $InsP_3R3$ in the presence of 2 μM $InsP_3$ and 0.5 mM ATP. Because most of the experiments resulted in multichannel bilayers, the *Po* values in each experiment were normalized to the maximal *Po* in the same experiment as described in Materials and Methods, and the normalized data from different experiments with each $InsP_3R$ isoform were averaged together for presentation and analysis. In agreement with our previous findings (Nosyreva et al., 2002; Tu

et al., 2002, 2003), $InsP_3R1$ expressed in Sf9 cells (RT1) display bell-shaped Ca^{2+} dependence with the peak at 257 nM Ca^{2+} (Fig. 1, *open circles*). Fit to the RT1 Ca^{2+} dependence using Eq. 1 (Fig. 1, *curve*; $R^2 = 0.99$) yielded apparent affinities of activating (K_{Ca}) and inhibitory (k_{Ca}) sites equal to 0.17 ± 0.03 μM Ca^{2+} and 0.37 ± 0.01 μM Ca^{2+}, respectively (Table 1). Similar to RT1, RT2 and RT3 also displayed bell-shaped Ca^{2+} dependence in the physiological range of Ca^{2+} concentrations (pCa 8–5). The peak of bell-shaped Ca^{2+} dependence was located at 154 nM Ca^{2+} for RT2 (Fig. 1, *solid triangles*), and at 107 nM Ca^{2+} for RT3 (Fig. 1, *solid circles*). Fit to the RT2 and RT3 Ca^{2+} dependence using Eq. 1 (Fig. 1, *curves*; $R^2 = 0.98$ for RT2 and $R^2 = 0.94$ for RT3) yielded the apparent affinities of the activating and inhibitory sites equal to 0.15 ± 0.04 μM Ca^{2+} and 0.16 ± 0.04 μM Ca^{2+} for RT2, and 0.06 ± 0.03 μM Ca^{2+} and 0.17 ± 0.02 μM Ca^{2+} for RT3, respectively (Table 1).

As described in the accompanying article (Tu et al., 2005), 5 mM concentration of ATP is required to maximally activate RT3 channels. Thus, in the next series of experiments we determined Ca^{2+} dependence of RT3 in the presence of 2 μM $InsP_3$ and 5 mM ATP. We found that in the presence of 5 mM ATP, RT3 displayed a ''square-shaped'' Ca^{2+} dependence with the maximal channel activity observed in the range of Ca^{2+} concentrations between 0.1 μM Ca^{2+} and 10 μM Ca^{2+} (pCa 7–5) (Fig. 2, *solid circles*). The ''square-shaped'' Ca^{2+} dependence observed in this condition is similar to ''square-shaped'' Ca^{2+} dependence described for *Xenopus* $InsP_3R$ ($InsP_3R1$) (Mak et al., 1998) and rat $InsP_3R3$ expressed in *Xenopus* oocytes (Mak et al., 2001b). Thus, to fit these data we used ''biphasic Hill equation'' (Eq. 2) adapted from Mak et al. (1998). Fit to RT3 Ca^{2+}-dependence data using Eq. 2 (Fig. 2, *thick curve*; $R^2 = 0.93$) yielded apparent affinities of activating and inhibitory sites equal to 0.029 ± 0.004 μM Ca^{2+} and 37 ± 6 μM Ca^{2+}

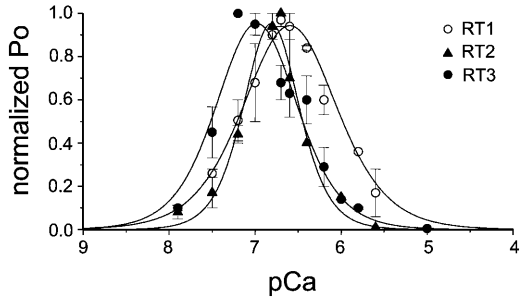

FIGURE 1 Ca^{2+} dependence of mammalian $InsP_3R$ isoforms. The single-channel open probability (*Po*) for each $InsP_3R$ isoform was measured as a function of cytosolic Ca^{2+} concentrations from 10 nM to 5 μM Ca^{2+} on the *cis* (cytoplasmic) side of the membrane in the presence of 2 μM $InsP_3$ and 0.5 mM Na_2ATP. The normalized and averaged data (see Materials and Methods) at each Ca^{2+} concentration are shown as means ± SE ($n \geq 3$) for RT1 (○), RT2 (▲), RT3 (●). These data were fitted by Eq. 1 (see Materials and Methods). The parameters of the best fit (*curves*) are in Table 1.

(Table 1). Thus, increase in ATP concentration to 5 mM had only a twofold effect on the apparent affinity of the Ca^{2+}-activating site of $InsP_3R3$, but resulted in a >200-fold reduction in the apparent affinity of the Ca^{2+}-inhibitory site of $InsP_3R3$ (Table 1). In contrast to $InsP_3R3$ (Fig. 2), we found that the Ca^{2+} dependence of $InsP_3R1$ and $InsP_3R2$ was not significantly different at 0.5 mM ATP and at 5 mM ATP (data not shown).

Ca^{2+} binding to $InsP_3R$ Ca^{2+} sensor

Different Ca^{2+} sensitivity of $InsP_3R1$, $InsP_3R2$, and $InsP_3R3$ has been observed in our experiments performed at 2 μM $InsP_3$ and 0.5 mM ATP (Fig. 1; Table 1). We previously proposed that the putative Ca^{2+} sensor region (Cas) in the coupling domain of $InsP_3R1$ is responsible for $InsP_3R1$ modulation by Ca^{2+} (Miyakawa et al., 2001; Tu et al., 2003). If ''Ca^{2+} sensor hypothesis'' is correct, then the differences in Ca^{2+} sensitivity between $InsP_3R$ isoforms should correlate with the differences in Ca^{2+} affinities of corresponding Cas regions. To test this prediction, we expressed in bacteria and purified RT1-Cas (E1932-R2270 of rat $InsP_3R1$), RT2-Cas (E1884-R2224 of rat $InsP_3R2$), and RT3-Cas (M1835-R2199 of rat $InsP_3R3$) proteins (Fig. 3 *A*). Similar yield of RT-Cas proteins was obtained as a result of our expression and purification procedure for each $InsP_3R$ isoform (Fig. 3 *B*).

Sequence alignment of RT1-Cas, RT2-Cas, and RT3-Cas regions shows a high degree of sequence conservation (Fig. 4). The E2100 glutamate residue that we previously identified to be critical for $InsP_3R1$ modulation by Ca^{2+} (Miyakawa et al., 2001; Tu et al., 2003) is conserved in $InsP_3R2$ (E2053) and $InsP_3R3$ (E2004) sequences (Fig. 4, *arrow*). In the previous study (Tu et al., 2003), we utilized intrinsic tryptophan fluorescence assay to compare Ca^{2+} binding affinity of RT1-Cas wild type and E2100 mutants. The W2255 and W2267 residues of $InsP_3R1$ present within the RT1-Cas region (Fig. 4, *open arrows*) are conserved in $InsP_3R2$ (W2209 and W2221) and in $InsP_3R3$ (W2183 and W2195). For all three $InsP_3R$ isoforms, these are the only two tryptophan residues within Cas sequence (Fig. 4). Thus, we reasoned that intrinsic tryptophan fluorescence of RT2-Cas and RT3-Cas proteins is likely to be quenched in a Ca^{2+}-dependent manner similar to our previous findings with RT1-Cas (Tu et al., 2003).

To test this hypothesis, we collected emission spectra (excitation at 280 nm) of RT1-Cas, RT2-Cas, and RT3-Cas proteins at different Ca^{2+} concentrations (pCa 9.4–2.0, buffered by 1 mM EGTA and 1 mM HEDTA). We found that the position of the emission peak (λ_{max}) remained constant at 332 nm for all three RT-Cas proteins at all Ca^{2+} concentrations (Fig. 5, *A–C*). However, a systematic and saturable change in the intensity of the intrinsic fluorescent signal was observed for all three RT-Cas proteins as a function of Ca^{2+} (Fig. 5, *A–C*). To compare the data

TABLE 1 Ca^{2+} dependence of mammalian $InsP_3R$ isoforms and Ca^{2+} sensor swap chimeras

	Ca^{2+} dependence					Ca^{2+} binding	
$InsP_3R$	ATP (mM)	Activation K_{Ca} (μM)	Inhibition k_{Ca} (μM)	Hill coefficient n_{Hill}	Peak (nM Ca^{2+})	K_{Ca} (μM)	Hill coefficient n_{Hill}
RT1	0.5	0.17 ± 0.03	0.37 ± 0.01	1.23	257	0.23 ± 0.04	0.47
RT2	0.5	0.15 ± 0.04	0.16 ± 0.04	2.05	154	0.16 ± 0.06	0.37
RT3	0.5	0.06 ± 0.03	0.17 ± 0.02	1.46	107	0.10 ± 0.04	0.39
	5	0.029 ± 0.004	37 ± 6	1.80 (*Ha*) 1.17 (*Hi*)	100–10,000		
RT1-V-3	0.5	0.06 ± 0.02	0.16 ± 0.01	2.17	100	RT3	RT3
	5	0.04 ± 0.003	33 ± 5	4.0 (*Ha*) 1.8 (*Hi*)	100–10,000		
RT3-V-1	0.5	0.24 ± 0.01	0.25 ± 0.02	1.65	239	RT1	RT1
	5	0.28 ± 0.03	0.31 ± 0.04	0.94	310		

Entries in the "Ca^{2+} binding" columns for RT1-V-3 and RT3-V-1 chimeras are used to indicate the "parental" $InsP_3R$ isoform for the Cas region in each chimera. Both *Ha* and *Hi* values (see Eq. 2) are entered in the n_{Hill} column for RT3 Ca^{2+} dependence at 5 mM ATP.

from different experiments, the observed changes in RT1-Cas, RT2-Cas, and RT3-Cas peak fluorescence intensity (ΔF) were corrected for dilution (see Materials and Methods), normalized to the maximal change in the peak fluorescence intensity (ΔF_{max}), averaged, and plotted against Ca^{2+} concentration (Fig. 6). By fitting the obtained results using Eq. 3 (see Materials and Methods) (Fig. 6, *curves*; $R^2 = 1.0$ for RT1-Cas, $R^2 = 0.99$ for RT2-Cas, and $R^2 = 0.98$ for RT3-Cas), we determined that the apparent affinity for Ca^{2+} (K_{Ca}) is equal to 0.23 ± 0.04 μM for RT1-Cas, 0.16 ± 0.06 μM for RT2-Cas, and 0.10 ± 0.04 μM for RT3-Cas (Table 1). Obtained results are in quantitative agreement with the sensitivity of $InsP_3R$ isoforms to Ca^{2+} modulation determined in planar lipid bilayer experiments (Fig. 1; Table 1). For all three RT-Cas regions, the Hill coefficient (n_{Hill}) determined in Ca^{2+}-binding experiments was in the range 0.4–0.5 (Fig. 6; Table 1). As discussed previously for RT1-Cas (Tu et al., 2003), an apparent negative cooperativity in association of RT-Cas regions with Ca^{2+} may be due to multimerization of recombinant proteins during our measurements or due to the presence of multiple Ca^{2+} binding sites within the RT-Cas regions.

Functional analysis of $InsP_3R$ Ca^{2+} sensor swap chimeras

Is Cas region alone sufficient to determine $InsP_3R$ sensitivity to Ca^{2+}? To answer this question and to further test the "Ca^{2+} sensor hypothesis" (Miyakawa et al., 2001; Tu et al., 2003), we generated chimeric RT1-V-3 and RT3-V-1 baculoviruses by swapping Cas-containing regions between $InsP_3R1$ and $InsP_3R3$ (Fig. 7 *A*). The regions swapped in RT1-V-3 and RT3-V-1 chimeras had the same amino-terminal boundary (E1932 in $InsP_3R1$ and M1835 in $InsP_3R3$) as the soluble RT1-Cas and RT3-Cas constructs expressed in bacteria (see Fig. 4). To simplify the construction, the swapped regions were 43 amino acids longer on carboxy-termini than the soluble RT1-Cas and RT3-Cas constructs (to the middle of the second predicted transmembrane domain, L2312 in $InsP_3R1$ and F2242 of $InsP_3R3$) (see Fig. 4). As discussed in the accompanying article (Tu et al., 2005), coupling domain of $InsP_3R1$ contains high-affinity (ATPA) and low-affinity (ATPB) ATP-binding sites (Fig. 7 *A*). In contrast, coupling domain of $InsP_3R3$ contains only low-affinity (ATPB) ATP-binding site (Fig. 7 *A*). Cas regions of $InsP_3R1$ and $InsP_3R3$ include corresponding ATPB sites in their sequence (Fig. 4). Thus, RT1-V-3 chimera contains the high-affinity ATPA site from $InsP_3R1$ and the low-affinity ATPB site from $InsP_3R3$ (Fig. 7 *A*). In contrast, RT3-V-1 chimera contains only the low-affinity ATPB site from $InsP_3R1$ (Fig. 7 *A*). As discussed in the accompanying article (Tu et al., 2005), $InsP_3R1$ and $InsP_3R3$ differ dramatically in their sensitivity to ATP modulation. Thus, swapping Cas regions may affect not only Ca^{2+}, but also ATP dependence of parental constructs. Expression of RT1-V-3 and RT3-V-1 proteins in Sf9 cells was confirmed by Western blotting with anti-$InsP_3R1$ T443 antibodies (Fig. 7 *B*) and anti-$InsP_3R3$ affinity purified IB7124 antibodies (Fig. 7 *C*). The epitopes for T443 antibodies (Kaznacheyeva et al., 1998) and IB7124 anti-

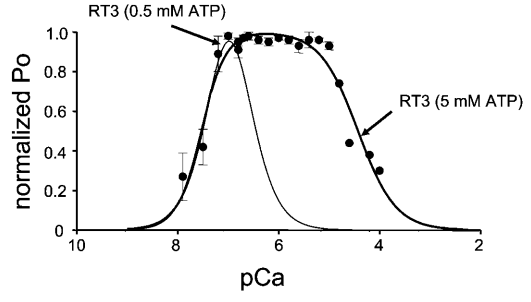

FIGURE 2 Ca^{2+} dependence of $InsP_3R3$ isoform at 5 mM ATP. The single-channel open probability (*Po*) for $InsP_3R3$ (RT3) was measured as a function of cytosolic Ca^{2+} concentrations from 10 nM to 100 μM Ca^{2+} on the *cis* (cytoplasmic) side of the membrane in the presence of 2 μM $InsP_3$ and 5 mM Na_2ATP. The normalized and averaged data (see Materials and Methods) at each Ca^{2+} concentration are shown as means ± SE ($n \geq 3$) (●). These data were fit by Eq. 2 (see Materials and Methods). The parameters of the best fit (*thick line*) are in Table 1. The fit to the RT3 Ca^{2+} dependence in the presence of 2 μM $InsP_3$ and 0.5 mM Na_2ATP (*thin line*) is from Fig 1.

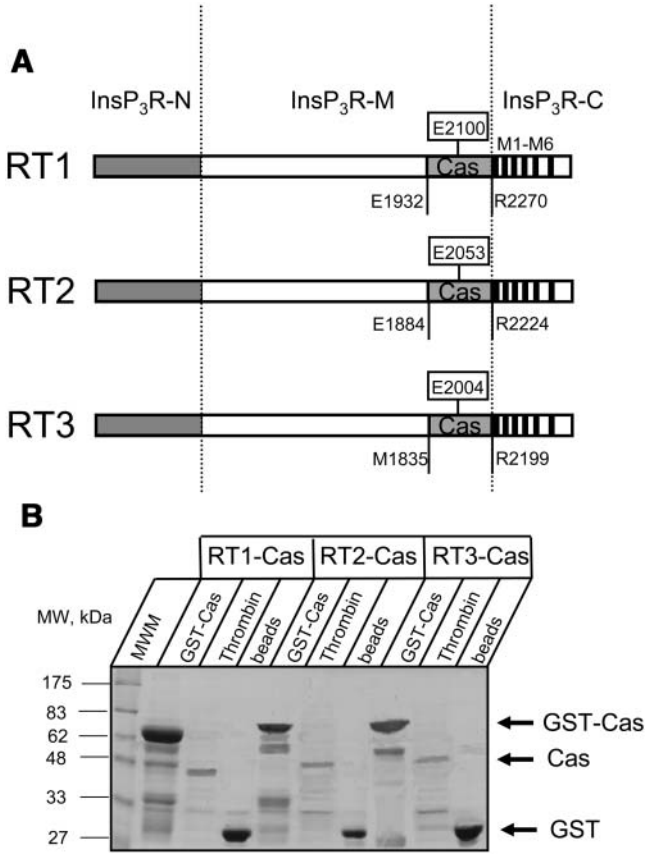

FIGURE 3 Expression and purification of the putative Ca^{2+} sensor (Cas) regions of mammalian $InsP_3R$ isoforms. (*A*) Domain structure of the $InsP_3R$ isoforms (adapted from Furuichi et al., 1994). The boundaries of the amino-terminal $InsP_3$ binding domain $InsP_3R$-N, the carboxyl-terminal channel-forming domain $InsP_3R$-C with transmembrane domains M1–M6, and the middle coupling domain $InsP_3R$-M are indicated. The putative $InsP_3R$ Ca^{2+} sensor region (*Cas*) is shown for $InsP_3R1$ (E1932-R2270), $InsP_3R2$ (E1884-R2224), and $InsP_3R3$ (M1835-R2199). (*B*) Expression and purification of the putative Ca^{2+} sensor (*Cas*) regions of mammalian $InsP_3R$ isoforms. Samples of GST-Cas attached to glutathione beads (*GST-Cas*), Cas proteins released by thrombin cleavage (*Thrombin*), and glutathione beads after thrombin cleavage (*beads*) were analyzed by SDS-PAGE gel electrophoresis (10% polyacrylamide gel stained with Coomassie blue). The predicted molecular weight of GST-Cas (68 kDa), Cas (39 kDa), and GST (29 kDa) are indicated by the arrows. Total protein of 1/60 (*GST-Cas* and *beads* lanes) or 1/200 (*Thrombin* lanes) was loaded on the gel for RT1-Cas, RT2-Cas, and RT3-Cas.

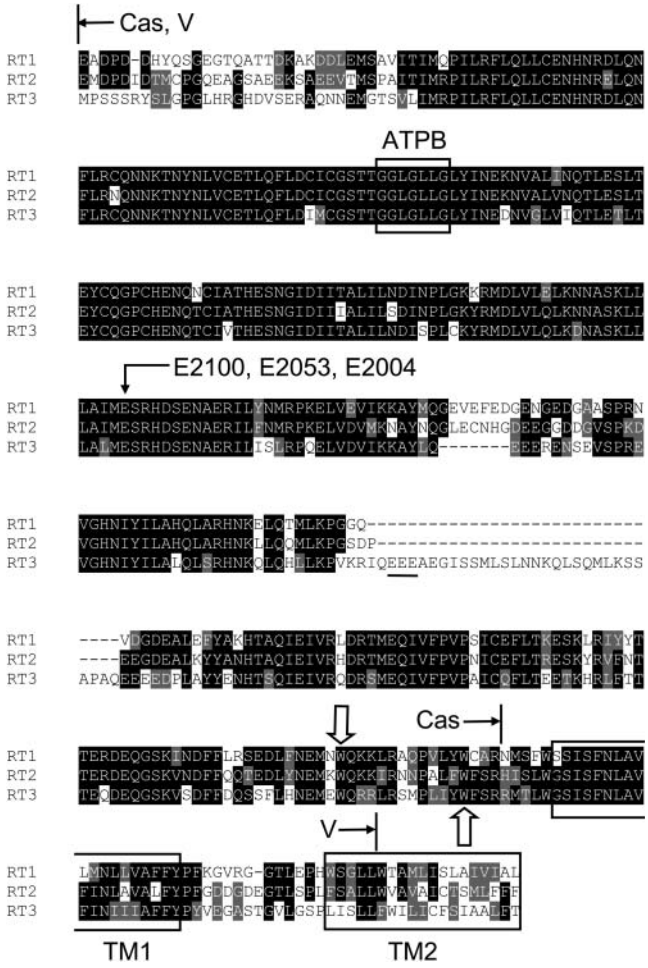

FIGURE 4 Sequence alignment of $InsP_3R$ Cas regions. The fragment of rat $InsP_3R1$ sequence (P29994, E1932-L2326) is aligned with the corresponding region of rat $InsP_3R2$ (P29995, E1884-F2281) and rat $InsP_3R3$ (Q63269, M1825-T2255). The amino-terminal boundary of the alignment (E1932 in $InsP_3R1$) is chosen from the limited trypsin digestion pattern of $InsP_3R1$ (Yoshikawa et al., 1999). The carboxy-terminal boundary of the alignment (L2326 in $InsP_3R1$) corresponds to the end of the predicted second transmembrane domain (*TM2*). The boundaries of soluble RT-Cas constructs (*Cas*) and the domain swap boundaries in RT1-V-3 and RT3-V-1 chimeras (*V*) are shown. Also shown is the ATPB binding site (^{2015}GGLGLLG^{2021} in $InsP_3R1$) (Maes et al., 2001), conserved glutamate residue (E2100 in $InsP_3R1$) mutated in our previous studies of $InsP_3R1$ Ca^{2+} sensor (Miyakawa et al., 2001; Tu et al., 2003), two conserved tryptophan residues (W2255 and W2267 in $InsP_3R1$) present within the RT-Cas region, a unique EEE cluster in the RT3-Cas sequence, and predicted boundaries of the TM1 and TM2 transmembrane domains.

bodies (Tu et al., 2005) are located at the carboxy-terminal ends of $InsP_3R1$ and $InsP_3R3$ sequences, which are not affected by swapping Cas-containing domains in RT1-V-3 and RT3-V-1 chimeras (Fig. 7 *A*).

Recombinant RT1-V-3 and RT3-V-1 chimeric proteins formed functional $InsP_3$-gated channels in planar lipid bilayers when recorded in standard recording conditions (pCa 6.7, 0.5 mM ATP, 2 μM $InsP_3$) (Figs. 8 *A* and 9 *A*). The Gaussian fit to the amplitude histogram of currents supported by RT1-V-3 chimera (Fig. 8 *B*) resulted in the average unitary current amplitude of RT1-V-3 channels equal to 1.86 $\pm$ 0.06 pA ($n = 3$) and the mean *Po* of RT1-V-3 channels equal to 20 $\pm$ 4% ($n = 3$). The open and closed dwell time distributions of RT1-V-3 channels could be fit with a single exponential function (Fig. 8, *C* and *D*) that yielded the mean open time of RT1-V-3 channels equal to 7.8 $\pm$ 0.9 ms ($n = 3$) and the mean closed time of RT1-V-3 channels equal to 10 $\pm$ 1 ms ($n = 3$). The Gaussian fit to the amplitude histogram of currents supported by RT3-V-1 chimera (Fig. 9 *B*) yielded the average unitary current amplitude equal to

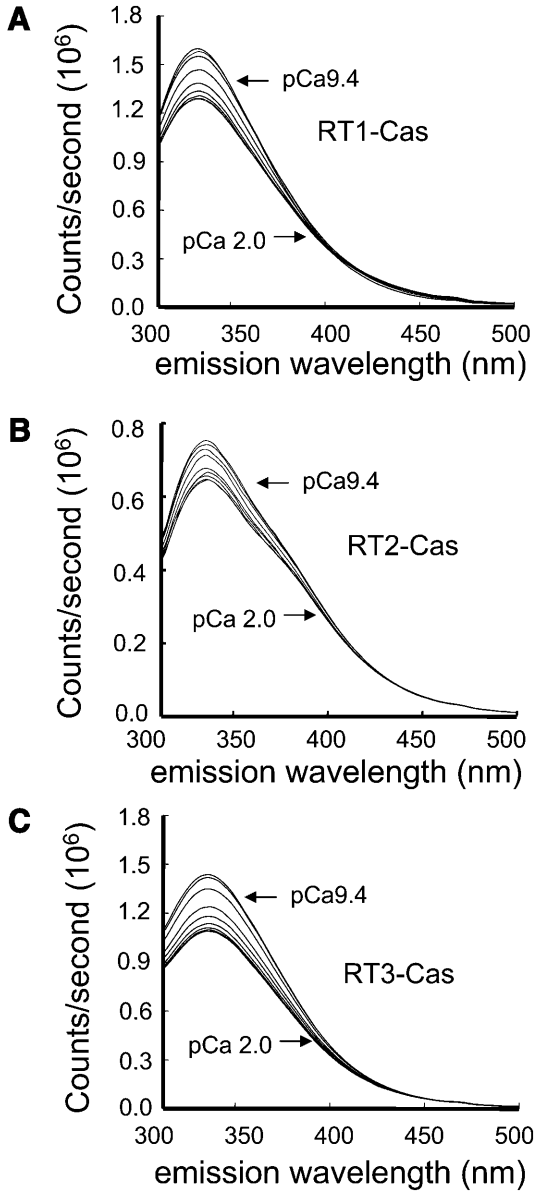

FIGURE 5 Intrinsic tryptophan fluorescence emission spectra of the $InsP_3R$ Ca^{2+} sensor region. Representative intrinsic tryptophan fluorescence emission spectra of RT1-Cas (*A*), RT2-Cas (*B*), and RT3-Cas (*C*) proteins at variable Ca^{2+} concentrations (pCa 9.4–2.0, as indicated). Similar results were obtained in at least three independent experiments with RT1-Cas, RT2-Cas, and RT3-Cas proteins.

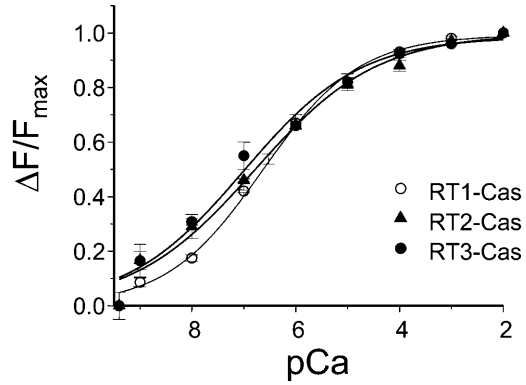

FIGURE 6 Ca^{2+} binding to the $InsP_3R$ Ca^{2+} sensor region. Dilution-corrected and normalized changes in the peak fluorescence intensity ($\Delta F/\Delta F_{max}$) were averaged together at each Ca^{2+} concentration (see Materials and Methods) and shown as means ± SE ($n \geq 3$) for RT1-Cas (○), RT2-Cas (▲), and RT3-Cas (●). The data for each $InsP_3R$ isoform were fitted by Eq. 3 (see Materials and Methods). The parameters of the optimal fits (*curves*) are presented in Table 1.

1.87 ± 0.06 pA ($n = 3$) and the mean *Po* equal to 8 ± 3% ($n = 3$). The open dwell time and closed dwell time distributions of RT3-V-1 currents were fit by a single exponential function (Fig. 9, *C* and *D*), resulting in the mean open time of RT3-V-1 channels equal to 8 ± 1 ms ($n = 3$) and the mean closed time equal to 83 ± 5 ($n = 3$). Thus, conductance and gating properties of RT1-V-3 and RT3-V-1 chimeric channels are similar to conductance and gating properties of wild-type $InsP_3R1$ and $InsP_3R3$ channels described in the accompanying article (Tu et al., 2005). Thus, we have not induced gross abnormalities in $InsP_3R$ gating and conductance properties by swapping Cas regions between $InsP_3R1$ and $InsP_3R3$.

We reasoned that low open probability of RT3-V-1 channels when compared with RT1-V-3 channels in standard recording conditions may be due to lower sensitivity of these channels to ATP modulation, as described for RT3 channels relative to RT1 channels in the accompanying article (Tu et al., 2005). To test this hypothesis, we compared channel activity of RT1-V-3 and RT3-V-1 chimeras in the presence of 2 μM $InsP_3$ at pCa 6.7 in the absence of ATP, at 0.5 mM ATP, and at 5 mM ATP (Fig. 10). We found that both RT1-V-3 and RT3-V-1 channels display very low levels of activity in the absence of ATP ($Po = 3 \pm 1\%$ ($n = 3$) for RT1-V-3 and $Po = 2 \pm 1\%$ ($n = 2$) for RT3-V-1) (Fig. 10, *A* and *B*, *top traces*). Addition of 0.5 mM ATP potentiated activity of RT1-V-3 channels to $Po = 20 \pm 4\%$ ($n = 3$) (Fig. 10 *A*, *middle trace*). The Po of RT3-V-1 channels at 0.5 mM ATP was much lower at 8 ± 3% ($n = 3$) (Fig. 10 *B*, *middle trace*). However, addition of 5 mM ATP resulted in maximal level of activity of both RT1-V-3 ($Po = 23 \pm 5\%$ ($n = 3$)) and RT3-V-1 ($Po = 25 \pm 7\%$ ($n = 2$)) channels (Fig. 10, *A* and *B*, *bottom traces*). Comparison with results in the accompanying article (Tu et al., 2005) clearly shows that RT1-V-3 channels are modulated by ATP similar to RT1 channels, and RT3-V-1 channels are modulated by ATP similar to RT3 channels. Thus, the main reason for differences in ATP sensitivity of the RT1 and RT3 channels is related to the presence or absence of the high-affinity ATPA site (Fig. 7 *A*), in agreement with our previous conclusions based on the functional analysis of $InsP_3R1$-*opt* mutant (Tu et al., 2002).

In the presence of 2 μM $InsP_3$ and 0.5 mM ATP both $InsP_3R1$ and $InsP_3R3$ display narrow bell-shaped Ca^{2+}

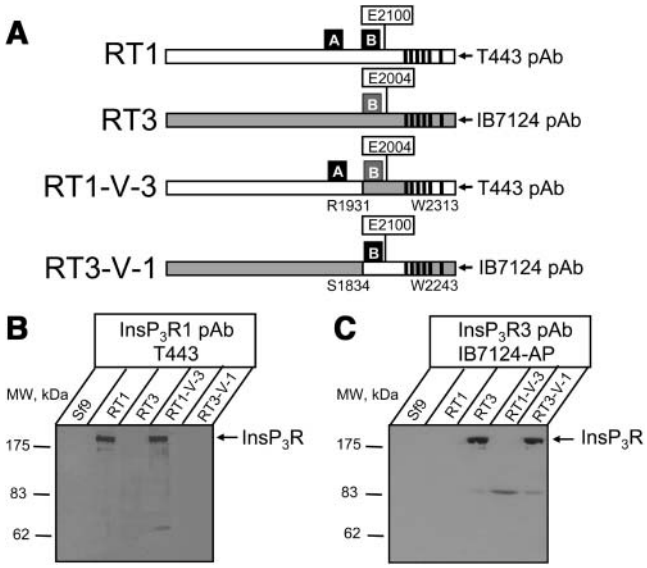

FIGURE 7 Expression of Ca^{2+} sensor swap chimeras. (*A*) The diagram of RT1, RT3, RT1-V-3, and RT3-V-1 constructs. In RT1-V-3 construct the putative $InsP_3R1$ Cas region (E1932-L2312) was replaced by the Cas region of $InsP_3R3$ (M1835-F2242; *shaded*). In RT3-V-1 construct the putative $InsP_3R3$ Cas region (M1835-F2242) was replaced by the Cas region of $InsP_3R1$ (E1932-L2312; *open*). Locations of E2100 residue in the $InsP_3R1$ Cas sequence (Miyakawa et al., 2001; Tu et al., 2003) and the corresponding E2004 residue in the $InsP_3R3$ sequence are shown. Also shown are locations of ATPA (^{1773}GGGGGGPG^{1780} in $InsP_3R1$) and ATPB (^{2015}GGLGLLG^{2021} in $InsP_3R1$ and ^{1919}GGLGLLG^{1925} in $InsP_3R3$) sites (Maes et al., 2001) and the epitopes for T443 (anti-$InsP_3R1$) (Kaznacheyeva et al., 1998) and IB7124 (anti-$InsP_3R3$) (Tu et al., 2005) polyclonal antibodies. (*B* and *C*) The microsomes isolated from noninfected Sf9 cells (*Sf9*), and from Sf9 cells infected with RT1, RT3, RT1-V-3, and RT3-V-1 baculoviruses were analyzed by Western blotting with anti-$InsP_3R1$ polyclonal antibody T443 (*B*) and anti-$InsP_3R3$ affinity purified polyclonal antibody IB7124-AP (*C*). For each microsomal preparation, 10 μg of total protein was loaded on the gel.

dependence with the peak at 257 nM Ca^{2+} for $InsP_3R1$ and 107 nM Ca^{2+} for $InsP_3R3$ (Fig. 1). To investigate the effects of Cas region swap on sensitivity of $InsP_3R$ to Ca^{2+}, we determined Ca^{2+} dependence of RT1-V-3 and RT3-V-1 channels in the same recording conditions. Because most of the experiments resulted in multichannel bilayers, the *Po* values in each experiment were normalized to the maximal *Po* in the same experiment as described in Materials and Methods and the normalized data from different experiments with each chimera were averaged together for presentation and analysis. We found that the RT1-V-3 chimera displayed bell-shaped Ca^{2+} dependence that closely overlaps with the RT3 Ca^{2+} dependence with the peak at 100 nM Ca^{2+} (Fig. 11 *A*, *solid circles*). Fit to the Ca^{2+} dependence of RT1-V-3 channels using Eq. 1 (Fig. 11 *A*, *smooth thick curve*; $R^2 = 0.98$) yielded the apparent affinities of activating and inhibitory Ca^{2+}-binding sites equal to 0.06 ± 0.02 and 0.16 ± 0.01 μM Ca^{2+} (Table 1), identical to the values obtained for the RT3 channels. The difference between RT1-V-3 and RT3 Ca^{2+}-dependence curves was due to differences in apparent Hill coefficients of Ca^{2+} modulation ($n = 2.17$ for RT1-V-3 and $n = 1.46$ for RT3; Table 1).

In contrast to RT1-V-3, the RT3-V-1 chimera displayed bell-shaped Ca^{2+} dependence that closely overlaps with the RT1 Ca^{2+} dependence with the peak at 239 nM Ca^{2+} (Fig. 11 *B*). Fit to the Ca^{2+} dependence of RT3-V-1 channels using Eq. 1 (Fig. 11 *B*, *smooth thick curve*; $R^2 = 0.99$) yielded the apparent affinities of activating and inhibitory Ca^{2+}-binding sites equal to 0.24 ± 0.01 and 0.25 ± 0.02 μM Ca^{2+} (Table 1), close to the values obtained for the RT1 channels. Similar to RT1-V-3 chimera, the difference between RT3-V-1 and RT1 Ca^{2+}-dependence curves was largely due to differences in apparent Hill coefficients of Ca^{2+} modulation ($n = 1.65$ for RT3-V-1 and $n = 1.23$ for RT1; Table 1). The results obtained with RT1-V-3 and RT3-V-1 chimeras (Fig. 11) indicated that swapping Cas regions between $InsP_3R1$ and $InsP_3R3$ was sufficient to exchange sensitivities to modulation by Ca^{2+} between these two mammalian $InsP_3R$ isoforms.

In the presence of 5 mM ATP, the RT3 channels display ''square-shaped'' Ca^{2+} dependence (Fig. 2). In the next series of experiments we compared Ca^{2+} dependence of RT1-V-3 and RT3-V-1 chimeras in the presence of 2 μM $InsP_3$ and 5 mM ATP. We found that in the presence of 5 mM ATP, RT1-V-3 chimera (Fig. 12, *open circles*) displayed a ''square-shaped'' Ca^{2+} dependence very similar to Ca^{2+} dependence of RT3 channels, whereas RT3-V-1 chimera (Fig. 12, *triangles*) displayed ''narrow'' Ca^{2+} dependence. Fit to the Ca^{2+} dependence of RT1-V-3 channels using Eq. 2 (Fig. 12, *smooth thick curve*; $R^2 = 0.98$) yielded the apparent afinities of activating and inhibitory Ca^{2+}-binding sites equal to 0.040 ± 0.003 and 33 ± 5 μM Ca^{2+} (Table 1), close to the values obtained for the RT3 channels at 5 mM ATP. Fit to the Ca^{2+} dependence of RT3-V-1 channels using Eq. 1 (Fig. 12, *smooth thick curve*; $R^2 = 0.96$) yielded the apparent affinities of activating and inhibitory Ca^{2+}-binding sites equal to 0.28 ± 0.03 and 0.31 ± 0.04 μM Ca^{2+} (Table 1), similar to the values obtained for the RT1 channels.

DISCUSSION

Ca^{2+} dependence of mammalian $InsP_3R$ isoforms

In standard recording conditions (2 μM $InsP_3$ and 0.5 mM ATP) all three mammalian $InsP_3R$ displayed narrow bell-shaped Ca^{2+} dependence within a physiological range of Ca^{2+} concentrations (pCa 8–5) (Fig. 1; Table 1). In an independent study we demonstrated that *Drosophila melanogaster* $InsP_3R$ displays similar narrow bell-shaped Ca^{2+} dependence when reconstituted into planar lipid bilayers and analyzed in standard recording conditions (Srikanth et al., 2004). Thus, bell-shaped Ca^{2+} dependence of $InsP_3R$ appears to be a fundamental and evolutionary conserved feature of all $InsP_3R$. This conclusion is in contrast with

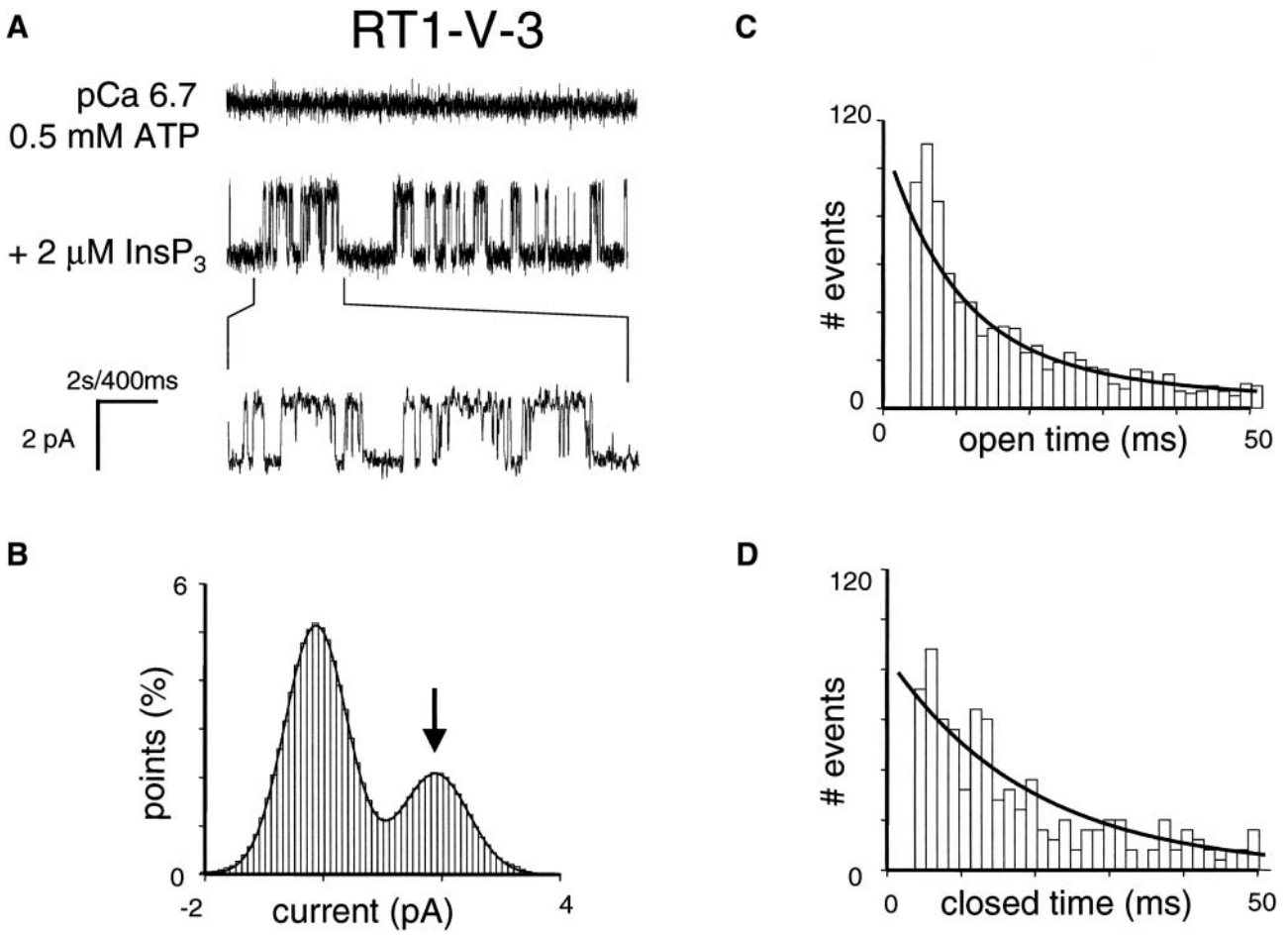

FIGURE 8 Functional properties of RT1-V-3 chimera. (*A*) Single-channel records of RT1-V-3 channels in planar lipid bilayers. The experiments were performed at pCa 6.7 in the presence of 0.5 mM ATP (control, *top trace*). Addition of 2 μM $InsP_3$ to the *cis* (cytoplasmic) side activates RT1-V-3 channels (*middle trace*). Current traces at the expanded timescale are also shown (*bottom trace*). (*B–D*) Analysis of the single-channel records of RT1-V-3 channels was performed and analyzed as described for $InsP_3R1$ in the accompanying article (Tu et al., 2005). The Gaussian peak corresponding to an open state of RT1-V-3 was centered at 1.89 pA, had $\sigma = 0.56$ pA, and area 28%. Open time distribution (*C*; number of events = 2200) was fitted with a single exponential function (*curve*) that yielded mean open time $\tau_0 = 8.4$ ms. Closed time distribution (*D*; number of events = 2200) was fitted with a single exponential function (*curve*) that yielded mean closed time $\tau_C = 9.8$ ms. The data from the same experiment with a single active channel in the bilayer were used for panels *A–D*.

some previous bilayer studies of $InsP_3R2$ (Ramos-Franco et al., 2000, 1998) and $InsP_3R3$ (Hagar et al., 1998). However, bell-shaped Ca^{2+} regulation of $InsP_3R3$ observed in our experiments is consistent with Ca^{2+} flux measurements in RIN-5F (Swatton et al., 1999) and 16HBE14o- bronchial mucosal cells (Missiaen et al., 1998) and with nuclear patch recordings of recombinant $InsP_3R3$ expressed in *Xenopus* oocytes (Mak et al., 2001b). The reasons for these discrepancies are not clear. The $InsP_3R1$ contain a high-affinity Ca^{2+}/calmodulin (CaM)-binding site in the coupling domain, which is not conserved in the $InsP_3R3$ sequence (Yamada et al., 1995). The fact that $InsP_3R3$ display bell-shaped Ca^{2+} dependence despite the absence of a Ca^{2+}/CaM-binding site further supports the notion that association with CaM at this Ca^{2+}/CaM binding site does not play a role in biphasic modulation of $InsP_3R$ by Ca^{2+} (Nosyreva et al., 2002; Zhang and Joseph, 2001) (but see Michikawa et al., 1999). With all three $InsP_3R$ isoforms displaying bell-shaped Ca^{2+} dependence (Fig. 1), how can we explain isoform-specific Ca^{2+} oscillation profiles observed in the study with DT40 cells (Miyakawa et al., 1999)? We would like to suggest that the unique ability of $InsP_3R2$ to support robust Ca^{2+} oscillations observed in the study of Miyakawa et al. (1999) results from higher affinity of $InsP_3R2$ for $InsP_3$ when compared to $InsP_3R1$ and $InsP_3R3$ isoforms (Miyakawa et al., 1999; Sudhof et al., 1991; Tu et al., 2005). We would like to suggest that ligation of B-cell receptors (BCR) with anti-BCR antibody in the study with DT40 cells (Miyakawa et al., 1999) resulted in long-lasting $InsP_3$ elevation above the threshold of $InsP_3R2$ activation, close to the threshold of $InsP_3R1$ activation, and below the threshold of $InsP_3R3$ activation.

The narrow shape of $InsP_3R1$ bell-shaped Ca^{2+} dependence in our planar lipid bilayer experiments (Fig. 1 and

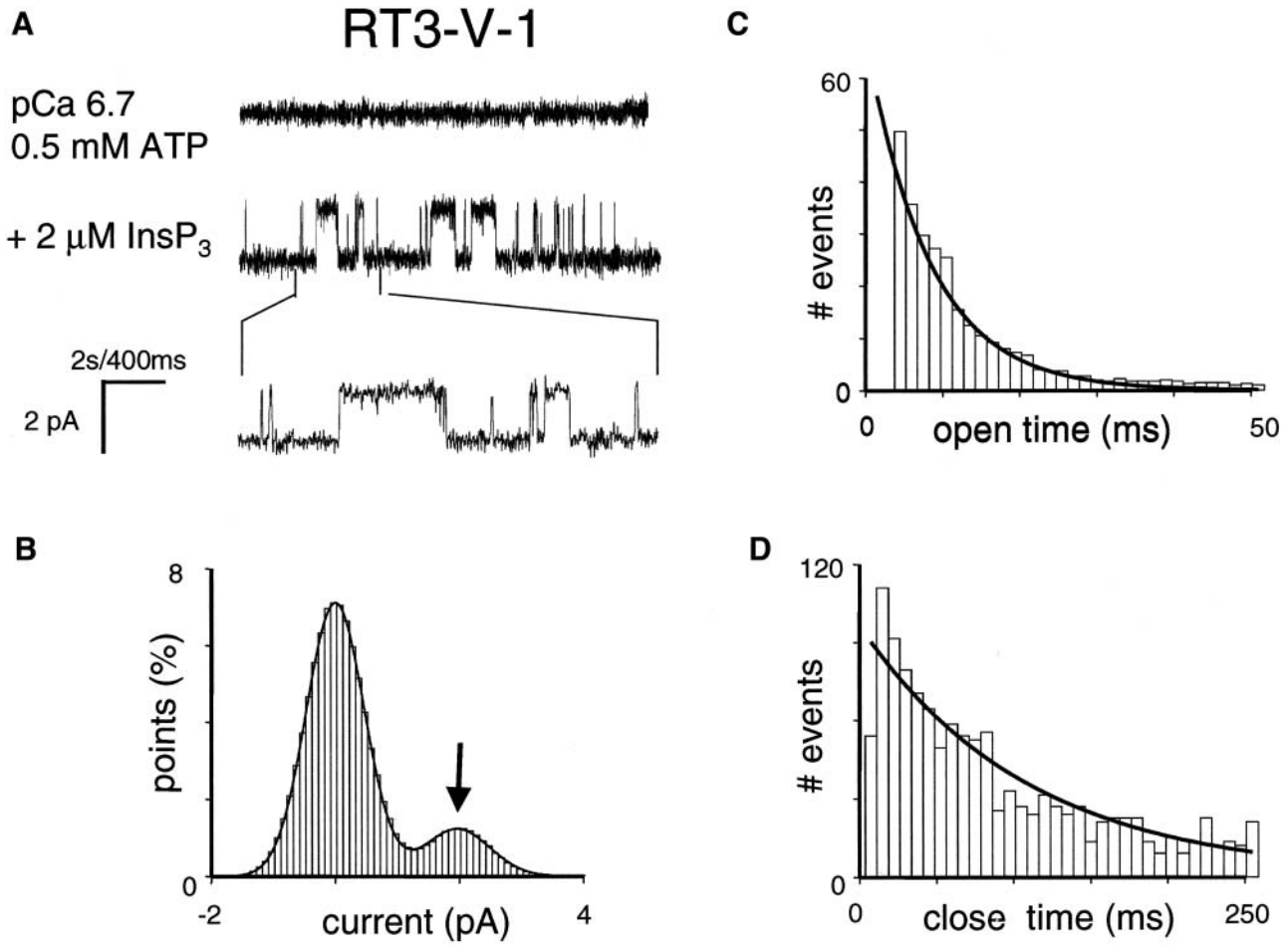

FIGURE 9 Functional properties of RT3-V-1 chimera. (*A*) Single-channel records of RT3-V-1 channels in planar lipid bilayers. The experiments were performed at pCa 6.7 in the presence of 0.5 mM ATP (control, *top trace*). Addition of 2 μM InsP3 to the *cis* (cytoplasmic) side activates RT3-V-1 channels (*middle trace*). Current traces at the expanded timescale are also shown (*bottom trace*). (*B–D*) Analysis of the single-channel records of RT3-V-1 channels was performed and analyzed as described for $InsP_3R3$ in the accompanying article (Tu et al., 2005). The Gaussian peak corresponding to an open state of RT3-V-1 was centered at 1.910 pA, had $\sigma = 0.53$ pA, and area 16%. Open and closed time distributions (*C* and *D*; number of events = 1000) were fitted with a single exponential function (*curve*) that yielded mean open time $\tau_0 = 8.4$ ms and mean closed time $\tau_C = 87.6$ ms for RT3-V-1. The data from the same experiment with a single active channel in the bilayer were used for panels *A–D*.

Nosyreva et al., 2002; Tu et al., 2002, 2003) is different from the ''square'' shape described for *Xenopus* $InsP_3R$ ($xInsP_3R$) ($InsP_3R1$ homolog; Kume et al., 1993) in nuclear patch experiments by Mak et al. (1998), but it is consistent with the earlier nuclear patch experiments by Stehno-Bittel et al. (1995). Also, the maximal *Po* of $InsP_3R1$ in our experiments (Tu et al., 2005) and in experiments by Stehno-Bittel et al. (1995) is in the range of 20–30%, whereas *Po* of $xInsP_3R$ in experiments of Mak et al. (1998) reaches 80%. What is an explanation of these differences? And more importantly, what behavior more closely reflects $InsP_3R1$ function in vivo? The *Po* of $InsP_3R1$ in vivo is unknown. However, all Ca^{2+} flux measurements performed with permeabilized cells (Iino, 1990), isolated brain microsomes (Finch et al., 1991), and *Xenopus* oocytes (Parker and Ivorra, 1990; Yao and Parker, 1992) are consistent with the ''narrow'' shape of $InsP_3R1$ Ca^{2+} dependence. In all of these experiments $InsP_3$-induced Ca^{2+} release was completely blocked by Ca^{2+} concentrations in the 5–10 μM range, whereas Ca^{2+} concentrations in the 50–100 μM range were required to inhibit $xInsP_3R$ and $InsP_3R3$ in nuclear patch recordings of Mak et al. (1998). Therefore, we concluded that ''narrow'' bell-shaped Ca^{2+} dependence observed in our experiments (Fig. 1 and Nosyreva et al., 2002; Tu et al., 2002, 2003) more closely reflects the physiological behavior of $InsP_3R1$ and $InsP_3R3$ than the ''square'' Ca^{2+} dependence of $xInsP_3R$ reported by Mak et al. (1998).

A recently published mathematical modeling study (Fraiman and Dawson, 2004) offers a potential explanation to the different behavior of $InsP_3R1$ observed in planar lipid bilayer experiments (Bezprozvanny et al., 1991 and Fig. 1) and in nuclear patch recordings (Mak et al., 1998). Fraiman and

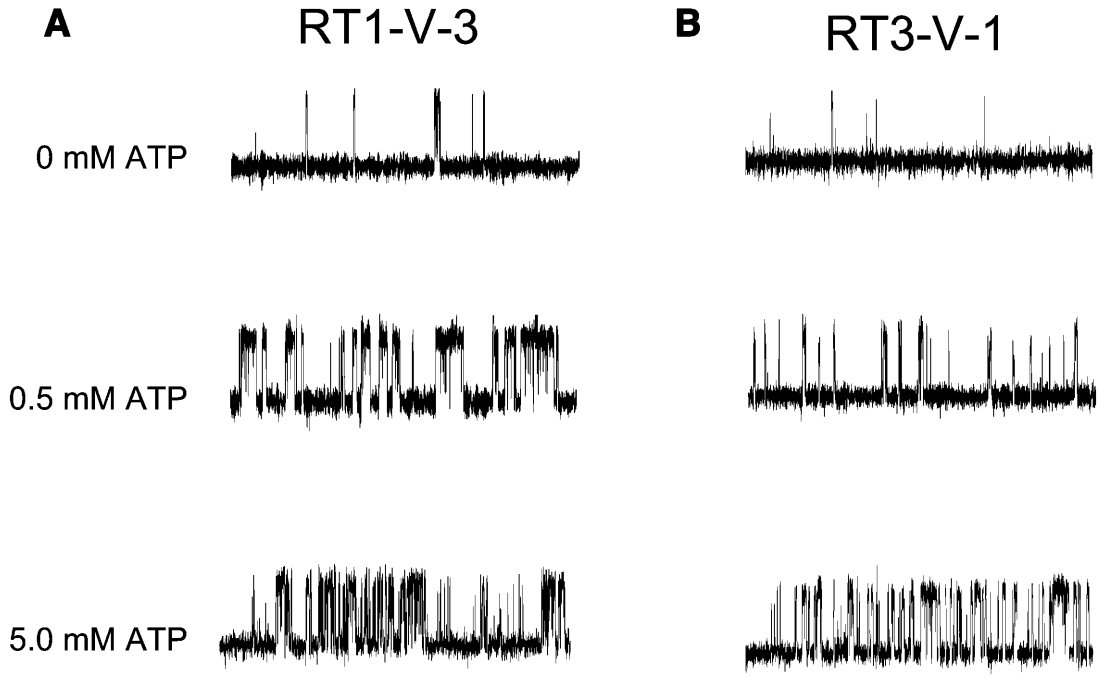

FIGURE 10 ATP sensitivity of Ca^{2+} sensor swap chimeras. Representative current records of RT1-V-3 (*A*) and RT3-V-1 (*B*) channels in the bilayers in the presence of 2 μM $InsP_3$ and pCa 6.7 at concentrations of Na_2ATP as indicated on the *cis* (cytoplasmic) side of the membrane. The recordings from the same experiment are shown on each panel. Similar results were obtained in at least three experiments with each chimera.

Dawson (2004) were able to explain most of the differences in results obtained in the planar lipid bilayer and nuclear patches recordings of $InsP_3R1$ activity by introducing an additional intraluminal Ca^{2+} modulatory site. These authors were able to explain ''square'' Ca^{2+} dependence and high *Po* of $xInsP_3R$ in nuclear patch recordings of Mak et al. (1998) by the fact that these experiments were performed using monovalent cations to carry current in the absence of Ca^{2+} or other divalent cations. In contrast, the planar lipid bilayer recordings are performed using 50 mM Ca^{2+} (Bezprozvanny et al., 1991) or Ba^{2+} (Fig. 1 and Nosyreva et al., 2002; Tu et al., 2002, 2003) as a current carrier. In the previous study we compared gating of $InsP_3R1$ with 50 mM Ca^{2+}, Ba^{2+}, Sr^{2+}, and Mg^{2+} as current carriers and analyzed modulation of $InsP_3R1$ by intraluminal Ca^{2+} levels (Bezprozvanny and Ehrlich, 1994). As discussed by Fraiman and Dawson (2004), the results from Bezprozvanny and Ehrlich (1994) are mostly consistent with the model proposed in their article. Thus, we concluded that ''square'' Ca^{2+} dependence and high *Po* of $xInsP_3R$ in nuclear patch recordings of Mak et al. (1998) most likely results from using divalent-free recording conditions (Fraiman and Dawson, 2004). Interestingly, this argument does not explain the difference between results of Mak et al. (1998) and Stehno-Bittel et al. (1995), as both groups used 140 mM K^+ as a current carrier in nuclear patch recordings of $xInsP_3R$ activity.

In standard recording conditions (2 μM $InsP_3$ and 0.5 mM ATP) $InsP_3R3$ also displayed narrow bell-shaped Ca^{2+} dependence in physiological range of Ca^{2+} concentrations (pCa 8–5) (Fig. 1; Table 1). In contrast to our experiments, Mak et al. reported ''square-shaped'' Ca^{2+} dependence of rat $InsP_3R3$ expressed in *Xenopus* oocytes and recorded in nuclear patch experiments in the presence of 0.5 mM ATP and 10 μM $InsP_3$ (Mak et al., 2001b). The maximal $InsP_3R3$ open probability in standard recording conditions in our experiments was low ($Po < 5\%$) (Tu et al., 2005), whereas *Po* of $InsP_3R3$ in experiments of Mak et al. (2001b) reaches 80%. Once again, ''narrow'' bell-shaped Ca^{2+} dependence of $InsP_3R3$ is consistent with Ca^{2+} flux measurements in permeabilized 16HBE14o- bronchial mucosal cells and RINm5F cells enriched in $InsP_3R3$ (Missiaen et al., 1998; Swatton et al., 1999). The explanation of the differences between ''narrow'' and ''square-shaped'' Ca^{2+} dependence of $InsP_3R3$ observed in our experiments (Fig. 1) and in experiments of Mak et al. (2001b) is most likely related to use of divalent-free recording conditions as discussed above for $InsP_3R1$.

Interestingly, the ''narrow'' Ca^{2+} dependence of $InsP_3R3$ in standard recording conditions (2 μM $InsP_3$ and 0.5 mM ATP) (Fig. 1) was converted to ''square-shaped'' Ca^{2+} dependence when recordings were performed in the presence of 2 μM $InsP_3$ and 5 mM ATP (Fig. 2). The ATP-induced change in the shape of Ca^{2+} dependence was a unique feature of $InsP_3R3$, as Ca^{2+} dependence of $InsP_3R1$ remained ''narrow'' in the presence of 5 mM ATP (data not shown). Fit to ''narrow'' (Fig. 1) and ''square'' (Fig. 2)

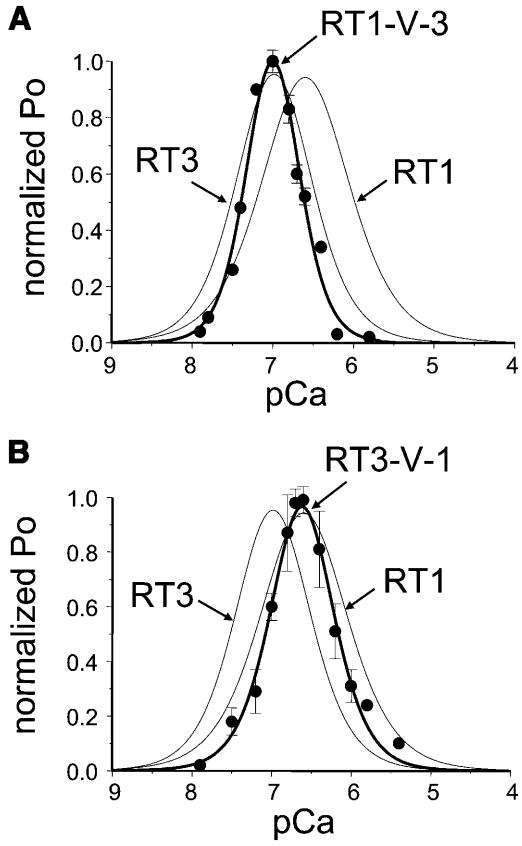

FIGURE 11 Ca^{2+} dependence of Ca^{2+} sensor swap chimeras at 0.5 mM ATP. Ca^{2+} dependence of RT1-V-3 (*A*) and RT3-V-1 (*B*) chimeras in planar lipid bilayers. The normalized and averaged data (see Materials and Methods) at each Ca^{2+} concentration are shown as means ± SE ($n \geq 3$) (●). The data were fit (*thick lines*) by Eq. 1 (see Materials and Methods). The parameters of the best fits are in Table 1. The fits to $InsP_3R1$ and $InsP_3R3$ (at 0.5 mM ATP) Ca^{2+} dependence curves (*thin lines*) are from Fig 1.

Ca^{2+}-dependence curves of $InsP_3R3$ indicated that an increase in ATP concentration from 0.5 to 5 mM resulted in a twofold increase in the apparent affinity of the Ca^{2+}-activating site of $InsP_3R3$ and a >200-fold reduction in the apparent affinity of the Ca^{2+}-inhibitory site of $InsP_3R3$ (Table 1). In experiments of Mak et al. (2001a) with $InsP_3R3$ expressed in *Xenopus* oocytes an increase in ATP concentration from 0 to 0.5 mM resulted in a 10-fold increase in the affinity of the Ca^{2+}-activating site and a threefold increase in the affinity of the Ca^{2+}-inhibitory site. Unfortunately, the inhibitory phase of $InsP_3R3$ Ca^{2+} dependence was not analyzed at ATP concentrations >0.5 mM by Mak et al. (2001a), so it is not clear if the differences between our studies and the Mak et al. studies are due to a different range of ATP concentrations compared (0.5 and 5 mM in our study and 0 and 0.5 mM in the Mak et al., 2001a study) or because of the use of divalent-free recording conditions as discussed above. Notably, Mak et al. (1998) earlier reported that the increase in $InsP_3$ concentration from 20 nM to 10 μM leads to a 280-fold reduction in the apparent affinity of the Ca^{2+}-

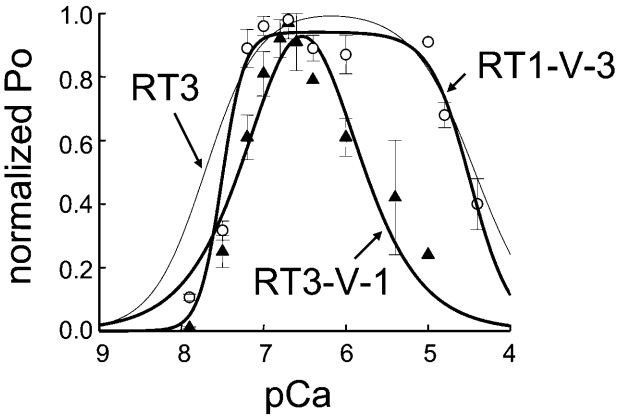

FIGURE 12 Ca^{2+} dependence of Ca^{2+} sensor swap chimeras at 5 mM ATP. Ca^{2+} dependence of RT1-V-3 (○) and RT3-V-1 (▲) chimeras in planar lipid bilayers at the presence of 5 mM ATP. The normalized and averaged data (see Materials and Methods) at each Ca^{2+} concentration are shown as means ± SE ($n \geq 3$). The RT1-V-3 data were fit by Eq. 2 (*thick curve*) and the RT3-V-1 data were fit by Eq. 1 (*thick curve*). The parameters of the best fits are in Table 1. The fit to Ca^{2+} dependence of $InsP_3R3$ at 5 mM ATP (*thin line*) is from Fig 2.

inhibitory site of $xInsP_3R$. In our hands the affinity of the $InsP_3R3$ Ca^{2+}-inhibitory site is affected in a very similar way by an increase in ATP concentration (Figs. 1 and 2; Table 1).

The role of $InsP_3R$ Ca^{2+} sensor

When modulation of different $InsP_3R$ isoforms by Ca^{2+} was compared side-by-side in standard recording conditions (2 μM $InsP_3$ and 0.5 mM ATP), we discovered that $InsP_3R3$ are most sensitive to modulation by Ca^{2+} (peak at 107 nM Ca^{2+}), followed by $InsP_3R2$ (peak at 154 nM Ca^{2+}), and then by $InsP_3R1$ (peak at 257 nM Ca^{2+}) (Fig. 1; Table 1). High sensitivity to activation by Ca^{2+} observed for $InsP_3R2$ is consistent with the previous Ca^{2+} flux studies in DT40 cells (Miyakawa et al., 1999) and with the single-channel recordings of native and recombinant $InsP_3R2$ (Ramos-Franco et al., 2000, 1998). High sensitivity to activation by Ca^{2+} observed for $InsP_3R3$ is also consistent with previous Ca^{2+} flux studies in DT40 cells (Miyakawa et al., 1999) and with single-channel recordings of recombinant $InsP_3R3$ expressed in *Xenopus* oocytes (Mak et al., 2001b).

In the previous studies (Miyakawa et al., 2001; Tu et al., 2003) we identified a putative Ca^{2+} sensor (Cas) region in the $InsP_3R1$ sequence. The sequence of Cas region is highly conserved between $InsP_3R$ isoforms (Fig. 4), including a conserved glutamate residue (E2100 in $InsP_3R1$), the importance of which we established previously (Miyakawa et al., 2001; Tu et al., 2003). Are small variations in Cas sequence (Fig. 4) sufficient to explain different Ca^{2+} sensitivity of $InsP_3R$ isoforms? To answer this question, we expressed RT1-Cas, RT2-Cas, and RT3-Cas proteins in

bacteria (Fig. 3) and performed a series of intrinsic tryptophan fluorescence measurements at different Ca^{2+} concentrations by following a method described previously for RT1-Cas (Tu et al., 2003). Importantly, the W2255 and W2267 residues of $InsP_3R1$ present within the RT1-Cas region (Fig. 4, *open arrows*) are conserved in $InsP_3R2$ and $InsP_3R3$. For all three RT-Cas proteins, the intensity of the intrinsic tryptophan fluorescence signal was quenched as a function of Ca^{2+} (Fig. 5), consistent with Ca^{2+}-induced conformational change. By fitting the obtained results we determined that the RT1-Cas apparent affinity for Ca^{2+} (K_{Ca}) is equal to 0.23 μM, RT2-Cas apparent affinity for Ca^{2+} is equal to 0.16 μM, and RT3-Cas apparent affinity for Ca^{2+} is equal to 0.10 μM (Fig. 6; Table 1). Thus, small variations in Cas sequence between different $InsP_3R$ isoforms (Fig. 4) do appear to be sufficient to result in different affinities for Ca^{2+} (Fig. 6). Future mutagenesis of the RT-Cas region or solution of the RT-Cas structure will be required to identify structural determinants that form a Ca^{2+}-binding site within the RT-Cas region.

Ca^{2+} binding affinities of isolated RT-Cas regions are in quantitative agreement with the sensitivity of corresponding $InsP_3R$ isoforms to the Ca^{2+} modulation determined in planar lipid bilayer experiments (Table 1). Are different RT-Cas affinities for Ca^{2+} sufficient to explain different Ca^{2+} sensitivity of $InsP_3R$ isoforms? To answer this question, we swapped Cas regions between the $InsP_3R1$ and $InsP_3R3$ isoforms and generated baculoviruses encoding RT1-V-3 and RT3-V-1 chimeras (Fig. 7). Single-channel analysis revealed that conductance and gating properties of RT1-V-3 and RT3-V-1 chimeras are similar to the properties of ''parental channels'' (Figs. 8 and 9). Thus, swapping $InsP_3R1$ and $InsP_3R3$ Cas regions did not induce gross abnormalities in $InsP_3R$ gating and conductance properties. The low-affinity ATP-binding site (ATPB) is contained within the Cas region (Fig. 4). Thus, RT1-V-3 chimera contains the ATPA site from $InsP_3R1$ and the ATPB site from $InsP_3R3$ (Fig. 7 *A*), and RT3-V-1 chimera contains the ATPB site from $InsP_3R1$ (Fig. 7 *A*). Consistent with the predominant role played by the ATPA site in modulating $InsP_3R1$ gating by ATP (Maes et al., 2001; Tu et al., 2002), RT1-V-3 chimera displayed ATP sensitivity similar to $InsP_3R1$ (Fig. 10 *A*) and RT3-V-1 chimera displayed ATP sensitivity similar to $InsP_3R3$ (Fig. 10 *B*).

Consistent with ''Ca^{2+} sensor hypothesis,'' we found that swapping Cas regions was sufficient to exchange Ca^{2+} sensitivities of $InsP_3R1$ and $InsP_3R3$ isoforms (Fig. 11, *A* and *B*; Table 1). Interestingly, both activating and inhibitory parts of bell-shaped Ca^{2+} dependence were affected by Cas domain swap in our experiments with RT1-V-3 and RT3-V-1 chimeras (Fig. 11, *A* and *B*). These results are consistent with our previous analysis of RT1-E2100 point mutants (Tu et al., 2003). As discussed in Tu et al. (2003), these data can be explained if Cas region forms a part of both Ca^{2+}-activating and Ca^{2+}-inhibitory sites, or by sequential Ca^{2+} binding to activating and inhibitory sites of the $InsP_3R$. In our experiments we found that the Ca^{2+} sensitivity of RT1-V-3 chimera closely resembles Ca^{2+} sensitivity of RT3 (Fig. 11 *A*), and the Ca^{2+} sensitivity of RT3-V-1 chimera closely matches Ca^{2+} sensitivity of RT1 (Fig. 11 *B*). Moreover, at 5 mM ATP RT1-V-3 chimera displayed ''square-shaped'' Ca^{2+} dependence similar to RT3, whereas RT3-V-1 chimera displayed ''narrow'' Ca^{2+} dependence similar to RT1 (Fig. 12). These results indicate that the features responsible for ATP-dependent transition from ''narrow'' to ''square'' Ca^{2+} dependence are uniquely encoded within RT3-Cas sequence.

Our results with RT1-V-3 and RT3-V-1 chimeras are in contrast to recent analysis of $InsP_3R1/2$ and $InsP_3R2/1$ coupling domain swap chimeras (Ramos et al., 2003). In the study of Ramos et al. (2003) Ca^{2+} sensitivity of 1-2-1 and 2-1-2 chimeras was largely lost and did not resemble Ca^{2+} sensitivity of either ''parental'' $InsP_3R$ (type 1 or type 2). Most likely explanation for the differences between our results and the results of Ramos et al. (2003) is related to the choice of boundaries for ''domain swap''. In our RT1-V-3 and RT3-V-1 constructs we choose domain swap boundaries (E1932 in $InsP_3R1$ and M1835 in $InsP_3R3$, Figs. 4 and 7 *A*) from the limited trypsin digestion pattern of $InsP_3R1$ (Yoshikawa et al., 1999), which also corresponds to the region of sequence divergence between $InsP_3R$ isoforms. In contrast, Ramos et al. (2003) choose the most conserved regions of the $InsP_3R1$ and $InsP_3R2$ sequences as boundaries for the coupling domain swap in 1-2-1 and 2-1-2 chimeras. Indeed, we obtained functional results similar to that of Ramos et al. (2003) with several other $InsP_3R3/1$ chimeric constructs with domain swap boundaries chosen in conserved regions of $InsP_3R1$ and $InsP_3R3$ sequences (data not shown).

Common and unique properties of mammalian $InsP_3R$ isoforms

In summary, data presented in this and the accompanying article (Tu et al., 2005) as well as the majority of the previously published reports indicate that all three mammalian $InsP_3R$ isoforms share common gating and conductance properties and display bell-shaped sensitivity to Ca^{2+} in a physiological range of Ca^{2+} concentrations (pCa 8–5). When compared to each other, the $InsP_3R1$ is a medium $InsP_3$-affinity, high ATP-affinity (no cooperativity), and low Ca^{2+}-affinity isoform; the $InsP_3R2$ is a high $InsP_3$-affinity, ATP-independent, medium Ca^{2+}-affinity isoform; the $InsP_3R3$ is a low $InsP_3$-affinity, low ATP-affinity (high cooperativity), and high Ca^{2+}-affinity isoform. Interestingly, saturation of the ATP binding site of $InsP_3R3$ (but not $InsP_3R1$) reduces apparent affinity of the Ca^{2+}-inhibitory site by >200-fold and converts ''narrow'' bell-shaped Ca^{2+} dependence of $InsP_3R3$ (Fig. 1) to ''square'' Ca^{2+} dependence (Fig. 2). It appears that high affinity of $InsP_3R2$ for

$InsP_3$ is encoded within the amino-terminal ligand-binding domain (Sudhof et al., 1991), high affinity of $InsP_3R1$ for ATP is due to the high-affinity ATPA binding site in the $InsP_3R1$ sequence (Fig. 10; also Maes et al., 2001; Tu et al., 2002), and the differences in Ca^{2+} sensitivity are encoded within a sequence of Ca^{2+} sensor (Cas) region (Figs. 4, 6, 11, and 12). These conclusions will be useful for understanding the mechanisms of $InsP_3R$ function and for analysis of Ca^{2+} signals supported by various $InsP_3R$ subtypes expressed in cells and tissues.

We are grateful to Gregory Mignery and Thomas C. Südhof for the kind gift of the rat $InsP_3R1$ and $InsP_3R2$ clones, to Graeme Bell for the kind gift of the rat $InsP_3R3$ clone, and to Humbert De Smedt for RT3 baculovirus. We thank Phyllis Foley for the administrative assistance and Elena Nosyreva for help with bilayer experiments.

This work was supported by the Welch Foundation and National Institutes of Health (R01 NS38082 to I.B.).

REFERENCES

Berridge, M. J. 1993. Inositol trisphosphate and calcium signalling. *Nature*. 361:315–325.

Bezprozvanny, I., and B. E. Ehrlich. 1994. Inositol (1,4,5)-trisphosphate ($InsP_3$)-gated Ca channels from cerebellum: conduction properties for divalent cations and regulation by intraluminal calcium. *J. Gen. Physiol.* 104:821–856.

Bezprozvanny, I., J. Watras, and B. E. Ehrlich. 1991. Bell-shaped calcium-response curves of $Ins(1,4,5)P_3$- and calcium-gated channels from endoplasmic reticulum of cerebellum. *Nature*. 351:751–754.

Fabiato, A. 1988. Computer programs for calculating total from specified free or free from specified total ionic concentrations in aqueous solutions containing multiple metals and ligands. *Methods Enzymol.* 157:378–417.

Finch, E. A., T. J. Turner, and S. M. Goldin. 1991. Calcium as a coagonist of inositol 1,4,5-trisphosphate-induced calcium release. *Science*. 252: 443–446.

Fraiman, D., and S. P. Dawson. 2004. A model of the IP3 receptor with a luminal calcium binding site: stochastic simulations and analysis. *Cell Calcium*. 35:403–413.

Furuichi, T., K. Kohda, A. Miyawaki, and K. Mikoshiba. 1994. Intracellular channels. *Curr. Opin. Neurobiol.* 4:294–303.

Hagar, R. E., A. D. Burgstahler, M. H. Nathanson, and B. E. Ehrlich. 1998. Type III InsP3 receptor channel stays open in the presence of increased calcium. *Nature*. 396:81–84.

Iino, M. 1990. Biphasic Ca^{2+} dependence of inositol 1,4,5-trisphosphate-induced Ca release in smooth muscle cells of the guinea pig *Taenia caeci*. *J. Gen. Physiol.* 95:1103–1122.

Kaznacheyeva, E., V. D. Lupu, and I. Bezprozvanny. 1998. Single-channel properties of inositol (1,4,5)-trisphosphate receptor heterologously expressed in HEK-293 cells. *J. Gen. Physiol.* 111:847–856.

Kume, S., A. Muto, J. Aruga, T. Nakagawa, T. Michikawa, T. Furuichi, S. Nakade, H. Okano, and K. Mikoshiba. 1993. The *Xenopus* IP_3 receptor: structure, function, and localization in oocytes and eggs. *Cell*. 73:555–570.

Maes, K., L. Missiaen, P. De Smet, S. Vanlingen, G. Callewaert, J. B. Parys, and H. De Smedt. 2000. Differential modulation of inositol 1,4,5-trisphosphate receptor type 1 and type 3 by ATP. *Cell Calcium*. 27:257–267.

Maes, K., L. Missiaen, J. B. Parys, P. De Smet, I. Sienaert, E. Waelkens, G. Callewaert, and H. De Smedt. 2001. Mapping of the ATP-binding sites on inositol 1,4,5-trisphosphate receptor type 1 and type 3 homotetramers by controlled proteolysis and photoaffinity labeling. *J. Biol. Chem.* 276:3492–3497.

Mak, D. O., S. McBride, and J. K. Foskett. 1998. Inositol 1,4,5-trisphosphate activation of inositol trisphosphate receptor Ca2+ channel by ligand tuning of Ca2+ inhibition. *Proc. Natl. Acad. Sci. USA*. 95:15821–15825.

Mak, D. O., S. McBride, and J. K. Foskett. 2001a. ATP regulation of recombinant type 3 inositol 1,4,5-trisphosphate receptor gating. *J. Gen. Physiol.* 117:447–456.

Mak, D. O., S. McBride, and J. K. Foskett. 2001b. Regulation by Ca2+ and inositol 1,4,5-trisphosphate (InsP3) of single recombinant type 3 InsP3 receptor channels. Ca2+ activation uniquely distinguishes types 1 and 3 InsP3 receptors. *J. Gen. Physiol.* 117:435–446.

Michikawa, T., J. Hirota, S. Kawano, M. Hiraoka, M. Yamada, T. Furuichi, and K. Mikoshiba. 1999. Calmodulin mediates calcium-dependent inactivation of the cerebellar type 1 inositol 1,4,5-trisphosphate receptor. *Neuron*. 23:799–808.

Missiaen, L., J. B. Parys, I. Sienaert, K. Maes, K. Kunzelmann, M. Takahashi, K. Tanzawa, and H. De Smedt. 1998. Functional properties of the type-3 InsP3 receptor in 16HBE14o- bronchial mucosal cells. *J. Biol. Chem.* 273:8983–8986.

Miyakawa, T., A. Maeda, T. Yamazawa, K. Hirose, T. Kurosaki, and M. Iino. 1999. Encoding of Ca2+ signals by differential expression of IP3 receptor subtypes. *EMBO J.* 18:1303–1308.

Miyakawa, T., A. Mizushima, K. Hirose, T. Yamazawa, I. Bezprozvanny, T. Kurosaki, and M. Iino. 2001. Ca(2+)-sensor region of IP(3) receptor controls intracellular Ca(2+) signaling. *EMBO J.* 20:1674–1680.

Nosyreva, E., T. Miyakawa, Z. Wang, L. Glouchankova, A. Mizushima, M. Iino, and I. Bezprozvanny. 2002. The high affinity calcium-calmodulin-binding site does not play a role in modulation of type 1 inositol (1,4,5)-trisphosphate receptor function by calcium and calmodulin. *Biochem. J.* 365:659–667.

Parker, I., and I. Ivorra. 1990. Inhibition by Ca^{2+} of inositol trisphosphate-mediated Ca^{2+} liberation: a possible mechanism for oscillatory release of Ca^{2+}. *Proc. Natl. Acad. Sci. USA*. 87:260–264.

Ramos, J., W. Jung, J. Ramos-Franco, G. A. Mignery, and M. Fill. 2003. Single channel function of inositol 1,4,5-trisphosphate receptor type-1 and -2 isoform domain-swap chimeras. *J. Gen. Physiol.* 121:399–411.

Ramos-Franco, J., D. Bare, S. Caenepeel, A. Nani, M. Fill, and G. Mignery. 2000. Single-channel function of recombinant type 2 inositol 1,4,5-trisphosphate receptor. *Biophys. J.* 79:1388–1399.

Ramos-Franco, J., M. Fill, and G. A. Mignery. 1998. Isoform-specific function of single inositol 1,4,5-trisphosphate receptor channels. *Biophys. J.* 75:834–839.

Srikanth, S., Z. Wang, H. Tu, S. Nair, M. K. Mathew, G. Hasan, and I. Bezprozvanny. 2004. Functional properties of the *Drosophila melanogaster* inositol 1,4,5-trisphosphate receptor mutants. *Biophys. J.* 86:3634–3646.

Stehno-Bittel, L., A. Luckhoff, and D. E. Clapham. 1995. Calcium release from the nucleus by $InsP_3$ receptor channels. *Neuron*. 14:163–167.

Sudhof, T. C., C. L. Newton, B. T. Archer, Y. A. Ushkaryov, and G. A. Mignery. 1991. Structure of a novel $InsP_3$ receptor. *EMBO J.* 10:3199–3206.

Swatton, J. E., S. A. Morris, T. J. Cardy, and C. W. Taylor. 1999. Type 3 inositol trisphosphate receptors in RINm5F cells are biphasically regulated by cytosolic Ca2+ and mediate quantal Ca2+ mobilization. *Biochem. J.* 344:55–60.

Taylor, C. W., A. A. Genazzani, and S. A. Morris. 1999. Expression of inositol trisphosphate receptors. *Cell Calcium*. 26:237–251.

Tu, H., T. Miyakawa, Z. Wang, L. Glouchankova, M. Iino, and I. Bezprozvanny. 2002. Functional characterization of the type 1 inositol 1,4,5-trisphosphate receptor coupling domain SII(+/−) splice variants and the *Opisthotonos* mutant form. *Biophys. J.* 82:1995–2004.

Tu, H., E. Nosyreva, T. Miyakawa, Z. Wang, A. Mizushima, M. Iino, and I. Bezprozvanny. 2003. Functional and biochemical analysis of the type 1 inositol (1,4,5)-trisphosphate receptor calcium sensor. *Biophys. J.* 85:290–299.

Tu, H., Z. Wang, E. Nosyreva, H. De Smedt, and I. Bezprozvanny. 2005. Functional characterization of mammalian inositol 1,4,5-trisphosphate receptor isoforms. *Biophys. J.* 88:1046–1055.

Ward, L. D. 1985. Measurement of ligand binding to proteins by fluorescence spectroscopy. *Methods Enzymol.* 117:400–414.

Yamada, M., A. Miyawaki, K. Saito, T. Nakajima, M. Yamamoto-Hino, Y. Ryo, T. Furuichi, and K. Mikoshiba. 1995. The calmodulin-binding domain in the mouse type 1 inositol 1,4,5-trisphosphate receptor. *Biochem. J.* 308:83–88.

Yao, Y., and I. Parker. 1992. Potentiation of inositol trisphosphate-induced Ca^{2+} mobilization in *Xenopus* oocytes by cytosolic Ca^{2+}. *J. Physiol.* 458:319–338.

Yoshikawa, F., H. Iwasaki, T. Michikawa, T. Furuichi, and K. Mikoshiba. 1999. Trypsinized cerebellar inositol 1,4,5-trisphosphate receptor. Structural and functional coupling of cleaved ligand binding and channel domains. *J. Biol. Chem.* 274:316–327.

Zhang, X., and S. K. Joseph. 2001. Effect of mutation of a calmodulin binding site on Ca2+ regulation of inositol trisphosphate receptors. *Biochem. J.* 360:395–400.